Crystallization of Silane-derived Synthetic Clay Minerals via SAXS

K.A. Carrado,[1] P. Thiyagarajan,[2] S. Seifert,[3] R. Kizilel[4]
[1]Chemistry Division, [2]Intense Pulsed Neutron Source, and [3]Advanced Photon Source (APS),
Argonne National Laboratory (ANL), Argonne, IL, U.S.A.
[4]Department of Chemical Engineering, Illinois Institute of Technology, Chicago, IL, U.S.A.

Introduction

Layered silicate mineral clays are of interest for basic research because of their applications to such diverse and technologically important fields as catalysis [1], ion-exchange [2], environmental issues [3], and organic-inorganic nano-com-posites [4]. This is especially true for the smectite clays, wherein a so-called 2:1 primary unit, consisting of two tetrahedral silicate layers that sandwich a central metal octahedral layer, is separated from another unit via electrostatic inter-actions that arise from exchangeable cations in hydrated interlayers. Hectorite is the layered magnesium silicate variant of a smectite clay [5].

A technique for making porous silicate heterogeneous catalysts from hectorite clay precursor sol gels was developed recently in our laboratories [6, 7]. A templating method was employed, in which organic molecules were used during clay crystallization, then removed via calcination. This results in a unique porous network. These materials have proven to be Co/Mo supports for hydro-desulfurization (HDS) catalysis [8]. Intensive efforts continue to create and control the pore size and porosity characteristics of clays in general, including pillared clay [9] and meso-structured clay (MSC) systems [6, 7, 10].

A rigorous examination of the crystallization process of MSC hectorites was undertaken recently by using ^{13}C magic-angle spinning nuclear magnetic resonance (MAS-NMR), ^{29}Si MAS-NMR, and small-angle x-ray scattering (SAXS) [11], as well as x-ray diffraction (XRD), thermogravimetric analysis (TGA), and atomic force microscopy (AFM) [12]. For comparison, a similar examination of a synthetic hectorite that was hydrothermally crystallized by using an organosilane as the silicon source is reported on here. The microstructure or extended network morphology of the MSC hectorites has not yet been identified, and it is believed that these characteristics would have the most effect on differences in catalytic behavior. Therefore, an in-depth analysis of nitrogen adsorption-desorption isotherm behavior, trans-mission electron microscopy (TEM) measure-ments, and contrast-matching small-angle neutron scattering (SANS) results of the various synthetic hectorites was undertaken toward this goal [13]. The SAXS data on the organosilane-derived clays are summarized here.

Methods and Materials

Our method [14] for *in situ* hydrothermal crystallization of silica-derived hectorite clays is to create a 2-wt% gel made of silica sol, magnesium hydroxide sol, lithium fluoride, and organic template and to reflux it in water for 2 days [6, 7]. For the silane-derived hectorite [15], the molar ratios of Si:Mg:Li in the sol gel are 0.5:1:0.25. A slurry of 1-wt% total solids in water is made by using LiF, a freshly prepared $Mg(OH)_2$ sol [6], and tetraethoxysilane [TEOS, $Si(OC_2H_5)_4$]. The slurries were refluxed vigorously for various amounts of time, then cooled, centrifuged, washed, and air-dried. This product is referred to as Li-(silane)-hectorite. Comparisons were made to Laponite RD, a synthetic hectorite obtained from Southern Clay Products in Gonzales, Texas.

The SAXS instrument was constructed at ANL and used on BESSRC undulator beamline ID-12 at the APS [16]. The SAXS data were collected in just 0.02- to 0.20-second exposures (scans), even with the use of an aluminum foil absorber. Mono-chromatic x-rays at 10.0 keV were scattered off the sample and collected on a nine-element mosaic change-coupled device (CCD) detector (15×15 cm^2) run at 1536×1536-pixel resolution. The same powder samples as those used for all analysis methods (XRD, TGA, NMR, etc.) were sprinkled onto and sealed in Scotch®, tape "cells." The scattered intensity was corr-ected for absorption, scattering from blank Scotch tape, and instrument background. The differential scattering cross section can be expressed as a function of the scattering vector Q, which is defined as $Q = (4\pi/\lambda)\sin\theta$, where λ is the wavelength of the x-rays and θ is the scattering half angle. The value of Q is proportional to the inverse of the length scale (Å^{-1}). The instru-ment was operated at a sample-to-detector distance of 391 cm for the range $0.007 < Q < 0.16$ Å^{-1}. Error bars are not shown in any of the figures for the sake of clarity; they are of equal or lesser size than the data points, except at high Q values.

Results

Previously, we monitored the crystallization of a silica-derived hectorite [11, 12]. Consistent data from SAXS, XRD, TGA, AFM, and infrared absorption spectroscopy (IR) from using quenched aliquots *ex situ* were obtained. All of these tech-niques discerned clay crystallites beginning to form within the first few hours

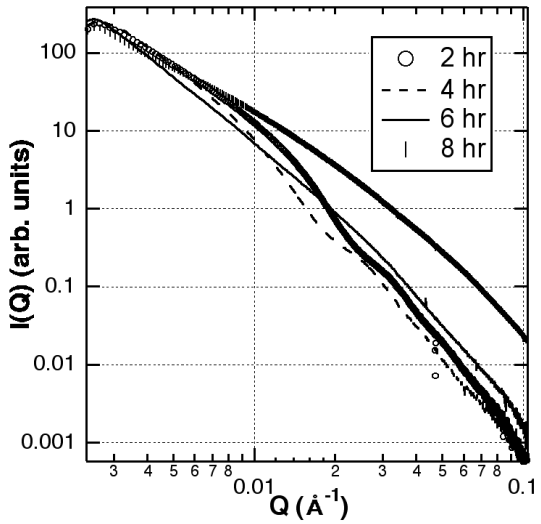

FIG. 1. SAXS of Li-(silane)-hectorite powder aliquots quenched at early crystallization times. Curves beyond 8 hours were very similar.

of reaction. ^{29}Si MAS-NMR displayed a clay silicate peak after just 1 hour. Solid-state ^{13}C NMR showed evidence of organo-clay formation in as little as 30 minutes and also revealed that 80% of the final organic loading was accom-plished in the first 10-12 hours. Up to 36 hours more are needed to incorporate the remaining 20% organic, indicating that a slower event dominates at the later stages of crystallization. The SAXS data showed this in progressively increasing power law values, indicating that more "open" structures condense into more dense structures with time, and this correlates with observed AFM images.

Figure 1 displays the SAXS data for Li-(silane)-hectorite powder aliquots, derived from using fresh TEOS, for 2-8 hours of crystallization time. The curves after 8 hours are very similar and are not shown for the sake of clarity. Dramatic differences in the SAXS data appear between 4 and 6 hours, when the peak at about Q = 0.03 Å^{-1} disappears. These results contrast with those of the other techniques, which showed more differences between 6 and 8 hours. Interestingly, the SAXS features are collectively quite different from the SAXS curves obtained for silica-derived hectorite [11].

Both silica- and silane-derived hectorites were imaged via TEM, and the electron diffraction patterns clearly show the presence of hectorite in both cases [13]. Two structural morphologies are present in the silica-derived sample: a 15- to 30-nm spherelike or disk-like phase, and one that is more traditionally consistent with the smectite morphology of long, thin, flexible plates. Since it is known that there is excess silica sol in these clays, the smaller phase is most likely due to spheres of the starting material, silica sol. There is a complete lack of smaller disks or spheres in the TEM images of silane-derived hectorites. The conclusion is that the silica-derived samples have a fairly wide range of clay particle sizes along with the presence of some silica sol, while the silane-derived clays display the larger, more uniform particle sizes that are more typical of natural hectorites.

Differences in surface textural properties are also borne out in the SAXS data. Curves for silica-hectorites are modeled best as "fractal aggregates of lamellae" [11], whereas the silane-hectorites do not model well to this equation. The silane-hectorites model better to the generic, unified exponential/power law approach developed by G. Beaucage [17], from which the specific fractal aggregates of lamellae equation are derived, without any specific parameters for lamellar disks. Figure 2 shows one representative fit as an example (the 48-hour sample data are very similar to the 90-hour sample data, especially at mid and high Q values). In this approach, one structural level includes both a Guinier regime and its corresponding power law regime. The fits here model best with two structural levels, each with their own resultant radius of gyration (Rg) values for the Guinier regime and power law exponents. For the first structural layer, the Rg was set arbitrarily to a very large value (1000 Å) to derive the power law exponent, which is 2.17; for the second structural layer, Rg = 143 Å (±0.4 Å), and the power law exponent is 3.32.

SANS is also a versatile technique for characterizing porous solid materials with high sensitivity on length scales of 1 to 100 nm. Morpho-logical information can be obtained by using the modified Guinier analysis for

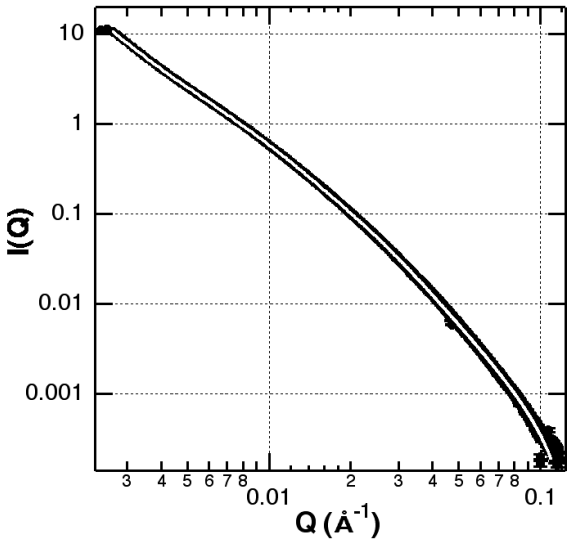

FIG. 2. SAXS of Li-(silane)-hectorite (90-hour sample) fitted over the entire range with the unified exponential/ power law equation [17] (white line) by using two layers. The reduced chi squared for this fit was 7.8.

sheetlike objects — a plot of $Q^2I(Q)$ versus Q^2. The presence of a linear region in such a plot at low Q indicates that the particles are lamellar. A notable feature in the modified Guinier plots for the clays is that, depending on the clay, the linear correlation breaks down at certain Q^2 values and the curve begins to fall off below these values. The bend-over region of the curve indicates that the lamellar particles have a finite lateral size, and the Q value corresponding to the bend-over region gives a qualitative idea of the lamellar lateral extent. Both the thicknessess and aspect ratios increase as laponite < silica-derived hectorite < Li-(silane)-hectorite < natural hectorite.

Discussion

A general view about the crystallization of hectorite has emerged. Initial clay nucleation begins with hydroxylated silica species condensing onto the pre-existing brucite sheets. At the same time, and during the LiF/brucite stirring period prior to silane addition, lithium (I) and magnesium (II) undergo isomorphous substitution. For silica-derived hectorite, this crystallization period takes 12 to 14 hours under these particular hydrothermal conditions. This time is substantially decreased for Li-(silane)-hectorites to 6 to 8 hours. Presumably this is because the silica sol needs time to dissolve and form the silicate precursor species that are immediately available when a silane is used. No matter which silicon source is employed, after the bulk of the crystallization is complete, optimization of layer-layer stacking and agglomeration of particles take place.

In terms of textural porosity, the silica-derived clay TEM images show micron-sized particles with highly "textured" or rough surfaces and with many flexible clay plates oriented outward in multiple directions on a small length scale (≈100 nm). These scaly, crackled surfaces give rise to an overall open morphology on a certain length scale. It is speculated that these features may result because of the silica sol impurity, which may physically keep small stacks of clay sheets apart and foster a smaller particle size. This open morphology does not occur with the larger silane-derived clay plates; they instead display a morphology much more typical of smectite clays. Both the thickness of clay tactoids and their aspect ratios are found to increase in SANS experiments as laponite < silica-derived hectorite < Li-(silane)-hectorite < natural hectorite.

Acknowledgments

This research was performed under the auspices of the U.S. Department of Energy (DOE), Office of Science, Office of Basic Energy Sciences (BES), through the Divisions of Chemical Sciences, Geosciences, and Biosciences (K.A. Carrado and S. Siefert) and Materials Science (P. Thiyagarajan). Use of the APS was supported by DOE BES under Contract No. W-31-109-ENG-38.

References

[1] J.P. Rupert, W.T. Granquist, and T.J. Pinnavaia, in *Chemistry of Clays and Clay Minerals*, edited by A.C.D. Newman (Longman Scientific & Technical, England, 1987), Chap. 6.
[2] H. Laudelout, in *Chemistry of Clays and Clay Minerals*, edited by A.C.D. Newman (Longman Scientific & Technical, England, 1987), Chap. 4.
[3] D.P. Siantar, B.A. Feinberg, and J.J. Fripiat, Clays Clay Miner. **42**, 187 (1994); P.B. Mitchell and K. Atkinson, Miner. Eng. 4, 1091 (1991).
[4] T.J. Pinnavaia and G. W. Beall, *Polymer-Clay Nanocomposites* (Wiley & Sons, England, 2000).
[5] R.E. Grim, *Clay Mineralogy* (McGraw-Hill, NY, 1968).
[6] K.A. Carrado, Appl. Clay Sci. **17**, 1 (2000).
[7] K.A. Carrado and L. Xu, Micropor. Mesopor. Mat., **27**, 87 (1999).
[8] K.A. Carrado, L. Xu, C.L. Marshall, D. Wei, S. Seifert, and C.A. Bloomquist, in *Nanoporous Materials II*, edited by A. Sayari, M. Jaroniec, and T.J. Pinnavaia (Elsevier, Amsterdam, 2000), p. 417; K.A. Carrado, C.L. Marshall, J.R. Brenner, and K. Song, Micropor. Mesopor. Mat. **20**, 17 (1998).
[9] J.T. Kloprogge, J. Porous Mat. **5**, 5 (1998).
[10] K. Torii, Y. Onodera, T. Iwasaki, M. Shirai, and M. Arai, J. Porous Mat. **4**, 261 (1997).
[11] K.A. Carrado, L. Xu, D.M. Gregory, K. Song, S. Seifert, and R.E. Botto, Chem. Mater. **12**, 3052 (2000).
[12] K.A. Carrado, P. Thiyagarajan, and K. Song, Clay Miner. **32**, 29 (1997); K.A. Carrado, G.W. Zajac, K. Song, and J.R. Brenner, Langmuir **13**, 2895 (1997).
[13] K.A. Carrado, R. Csencsits, P. Thiyagarajan, S. Seifert, S.M. Macha, and J.S. Harwood, J. Mater. Chem. **12**, 3228 (2002).
[14] K.A. Carrado, J.E. Forman, R.E. Botto, and R.E. Winans, Chem. Mater. **5**, 472 (1993); K.A. Carrado, Ind. Eng. Chem. Res. **31**, 1654 (1992).
[15] K.A. Carrado, L. Xu, R. Csencsits, and J.V. Muntean, Chem. Mater. **13**, 3766 (2001).
[16] For a full description of the instrument, see http://www.bessrc.aps.anl.
[17] G. Beaucage, J. Appl. Cryst. **28**, 717 (1995).